EUROPEAN ORGANIZATION FOR NUCLEAR RESEARCH

[Memorandum to the ISOLDE and Neutron Time-of-Flight Committee]

PUMA: antiprotons and radioactive nuclei

June 9, 2018

J. Carbonell[1,4], A. Corsi[1], F. Flavigny[4], H. De Gersem[7], G. Hupin[4], Y. Kubota[5], R. Lazauskas[3], S. Malbrunot[2], N. Marsic[7], W. F. O. Muller[7], S. Naimi[5], N. Nakatsuka[7], A. Obertelli[7], N. Paul[1], P. Pérez[1,2], E.C. Pollacco[1], M. Rosenbusch[5], R. Seki[6], T. Uesaka[5], F. Wienholtz[2]

[1] *CEA, IRFU, Université Paris-Saclay, France*
[2] *CERN, Geneva, Switzerland*
[3] *Institut Hubert Curien, CNRS, France*
[4] *Institut de Physique Nucléaire, Orsay, CNRS, France*
[5] *RIKEN Nishina Center, Wakoshi, Japan*
[6] *RCNP, Osaka, Japan*
[7] *Technische Universität Darmstadt, Germany*

Spokesperson: A. Obertelli, aobertelli@ikp.tu-darmstadt.de
Contact person: S. Malbrunot, stephan.ettenauer@cern.ch

Abstract: Antiprotons as a probe to study short-lived isotopes remain unexploited despite past pioneer works with stable nuclei. In particular, low-energy antiprotons are expected to offer a very unique sensitivity to the neutron and proton densities at the annihilation site, i.e. in the tail of the nuclear density. Such studies are the first motivation of the PUMA project which aims at transporting one billion antiprotons from CERN/ELENA to CERN/ISOLDE to perform the capture of low-energy antiprotons by short-lived nuclei.

In the present Addendum to a recent Letter of Intent [1], we report on the intended physics case of PUMA. The experimental methodology and theoretical developments to be undertaken in the coming years are presented. A short report on the ongoing and short-term technical developments for PUMA is also given.

Requested protons: [x] protons on target, (split into [y] runs over [z] years)
Experimental Area: [EAR1 or EAR2]

Contents

1 Antiprotons and nuclear structure

The first nuclear structure experiment with antiprotons was performed at Brookhaven National Laboratory, USA in the 1970s [2]. Low energy antiprotons were sent onto targets made of different solid materials (C, Ti, Ta, Pb) and charged pions from annihilation were measured in a bubble chamber where the targets were inserted. Since the electric charge is conserved during the annihilation process, the measurement of the ratio of positive and negative pions should be related to the annihilated proton-to-neutron ratio. Detection efficiency was considered in the analysis, as well as the difference of annihilation probability with protons and neutrons. The later correction term was estimated with ^{12}C as reference. The obtained normalised neutron-to-proton annihilation ratios show values significantly larger than N/Z for all cases. The relative excess compared to N/Z was interpreted as an excess of neutrons in the tail of the nuclear density and quantified as a so-called *halo factor*. In the case of ^{208}Pb, 2.3(5) times more neutron annihilations were observed compared to what one could expect from N/Z. Since this pioneer study, antiprotons have been used to investigate the nature of the tail of the nuclear density in stable nuclei.

The initial interpretation of this first work clearly suffered from the lack of a detailed treatment of final state interactions, as well as the lack of theoretical understanding for the site of the annihilation. These points were partly addressed in the interpretation of later works at CERN, where the annihilation process from nucleon- and nucleus-antiproton collisions were mostly studied, at the Low Energy Antiproton Ring (LEAR) and the Antiproton Decelerator (AD). The sensitivity of low-energy antiprotons to the very surface of nuclei was demonstrated [3], although a fully microscopic and consistent treatment of the antiproton-nucleus many-body problem still remains to be developed. The major part of nuclear structure studies with antiprotons relied on the detection of X rays from the decay of antiprotonic atoms [4, 5, 6] and γ rays from the residual nuclei [7, 8]. Several of these works aimed at determining the neutron skin thickness of stable nuclei.

As of today, no accelerator complex provides low-energy antiprotons to be used as probes for unstable nuclei. Indeed, the use of antiprotons with unstable nuclei requires two large scale facilities (one for the antiproton production and one for radioactive-ion beams (RIB)) connected together, or a way to bring antiprotons to a RIB facility. This was proposed for FAIR as the FLAIR project [9] but has not been included in the Start Version of FAIR. There is no RIB-antiproton collider today. The experiment detailed in the Letter of Intent and this addendum aims at bringing stored antiprotons from ELENA to the ISOLDE facility [10] at CERN. Its results may provide the necessary inputs to advocate for a low-energy antiproton-radioactive ion collider at CERN which, in return, may open new perspectives in studying nuclear ensembles.

2 Physics with PUMA

2.1 Neutron skins and halos

The occurrence of neutron halos was discovered in light-mass nuclei at the limit of nuclear existence, i.e. at the neutron drip line [11]. Halo nuclei exhibit a spatially extended wave function well beyond the core of the nucleus and represent a unique quantum phenomenon [12, 13] wherein the nucleon probability density lies mostly in the region forbidden by classical mechanics. While only s-wave halos have been observed so far, p-wave neutron halos have also been recently claimed to appear in very neutron rich Ne and Mg isotopes from breakup cross sections [14, 15]. A more direct measurement is needed to confirm these conclusions. For medium mass nuclei, the appearance of halos is predicted by several effective models with varying predictions from one to another [16, 17, 18, 19, 20]. Except some work within the Nilsson-level framework [21, 22, 23], the role of deformation has been barely studied so far and no data firmly support the existence of deformed halos. Neutron skins, corresponding to a neutron density higher than the proton density at the surface of the nucleus, have been evidenced in stable nuclei. Thick neutron skins, i.e. thicker than ~ 0.35 fm, were observed in light neutron rich nuclei. Microscopic models predict the development of thick neutron skins in very neutron rich medium mass nuclei but no experimental evidence exists so far. Such thick neutron skins would represent a unique occurrence of low-density pure neutron matter in the laboratory. but so far no quantitative evidence exists.

The nature of neutron skins in nuclei may not be as simple as described by mean field approaches. Parity-violating electron scattering analysis [24] as well as predictions from a data-constrained dispersive optical model analysis [25] favor thicker skins than *ab initio* predictions and most microscopic calculations, as well as compared to strong-probe extracted values [26, 27]. We still have a lot to learn about the nuclear surface properties. Spatial correlations including alpha clustering are predicted to take place at sub-saturation densities and therefore at the nuclear surface [28]. It is expected that clustering and the formation of inhomogeneous matter at low densities modifies the tail of the proton density. If such correlations are confirmed experimentally, it would modify our understanding of the symmetry energy of the nuclear equation of state, as compared to calculations assuming a uniform uncorrelated spatial distribution of constituents [29]. Recently *ab initio* calculations have been extended to medium mass nuclei but show the need for more data. Calculated binding energies and matter radii of stable nuclei show a systematic discrepancy compared to experiment when the coupling constants of the perturbative expansion of the input two- and three-body interactions up to the next-to-next-to-next leading order are fixed to scattering data and three-body nuclei, showing limitations to the most recent *ab initio* theories [30].

For the above reasons, the very tail of the nuclear density in neutron-rich isotopes has a strong interest, although difficult to access experimentally. The use of low-energy antiprotons as a probe may remedy this lack of experimental information. These studies were first proposed by Wada and Yamazaki in 2004 [31].

The first objectives of the PUMA experiment are (i) to provide a new observable that characterises the density tail of radioactive nuclei, (ii) to evidence new proton and neutron halos, (iii) to understand the development of neutron skins in medium-mass nuclei. The foreseen studies are expected to provide new information on the nuclear many-body problem, which may eventually shed light on our understanding of neutron(-rich) matter at low density.

Note that the observable PUMA will provide is the number of proton-to-neutron annihilations after antiproton capture. This quantity is to be connected to the proton-over-neutron density ratio integrated over the region of annihilation sites, i.e. in the tail on the nuclear radial density. PUMA is then complementary to measurements aiming at neutron-skin thickness determination and is sensitive to the outer part of the radial density distribution.

At this stage, several physics cases have been identified to be suitable for the investigation of the neutron and proton composition of the nuclear density tail in radioactive nuclei. They are summarized in Table 1. It is important to note that (i) reference measurements with stable nuclei will first be done at ELENA and will provide benchmark data for the response function of the device, as well as benchmarks for theory and the foreseen interpretation method, (ii) measurements along isotopic chains are believed to be important since they will allow studies which may provide more (relative) accuracy than individual measurements.

Nuclei	Objective
^{4,6,8}He, ^{7,9,11}Li	1) neutron skin and halos as a function of isospin
	2) (high statistics) study of annihilation process
^{8}B, ^{17,18}Ne	search for proton halos
$^{26-31}$Ne, ^{28,33}Mg	1) neutron skin in light isotopic chains
	2) search for (p-wave) neutron halos
$^{14-22}$O, $^{104-138}$Sn	1) evolution of neutron skins with isospin
	2) exclusive final state population (when gamma detection included)

Table 1: Foreseen first physics cases at ISOLDE. Among the raised cases, the most neutron-rich Ne, Mg and Sn isotopes may not be produced at enough rates for a possible measurement.

Next steps In the coming year (2019), extended simulations will be performed for each of the above cases considering their specificities (emittance, intensity, lifetime, efficiency) together with the final geometry of the PUMA apparatus. Expected statistics and accuracy for each physics case will be part of the forthcoming PUMA proposal. First details on the method and apparatus are given in this report.

2.2 Method

As stated in the earlier Letter of Intent [1], the PUMA project aims at transporting one billion antiprotons from CERN/ELENA to CERN/ISOLDE to perform the capture of low-energy antiprotons by short-lived nuclei.

The PUMA ion trap will consist of a storage trap (S trap) dedicated to the storage of a large amount of antiprotons, and a collision trap (C trap) dedicated to the interaction of antiprotons with unstable ions. Both zones will be located in a 4 T magnetic field provided by a superconducting solenoid.

A proposed operation scheme of the system is presented in Fig. 1. The scheme will consist of five key techniques: a pulsed drift tube (PDT) to slow down antiprotons and ions at the entrance of the double trap, a rotating wall excitation for the antiproton cloud shaping, sympathetic electron cooling, fractional extraction of antiprotons from the reservoir, and nesting to trap oppositely charge ions in the same region. Details on the devices to be built, the current situation of the project and agenda are given in section 3.
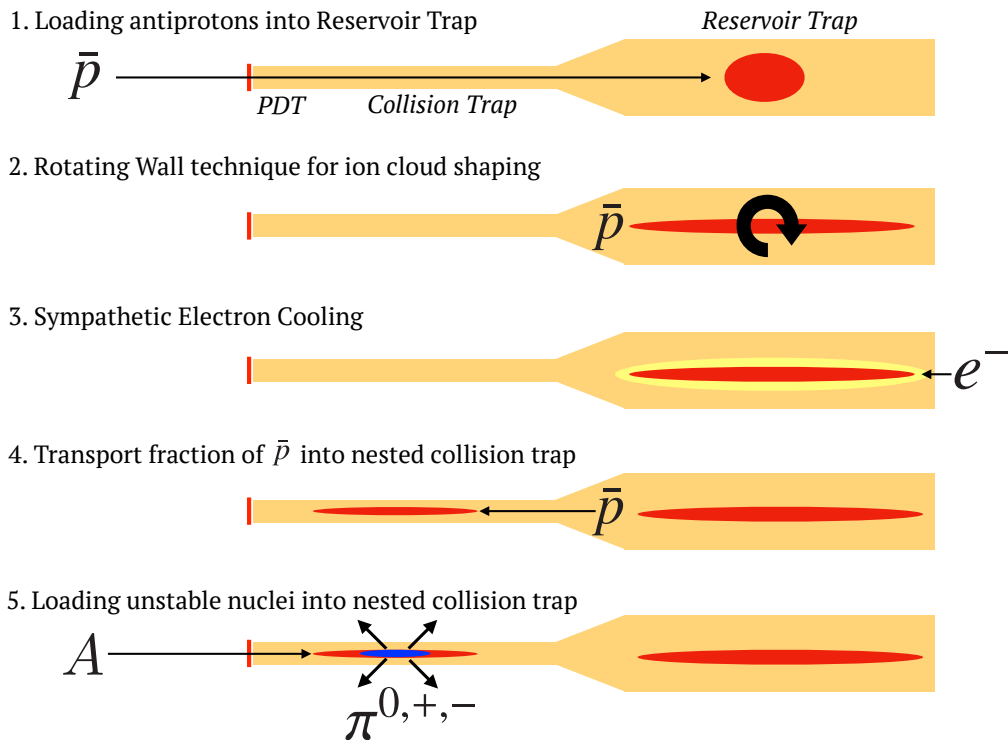

Figure 1: Operation scheme of PUMA.

The annihilation probability of an individual nucleus with stored antiprotons is estimated to reach 10^6 barns at 100 eV relative energy [32]. Antiprotons annihilate with both protons and neutrons. The quasi-totality of decay channels are composed of energetic pions with conservation of the initial charge and momentum of the antiproton-nucleon

system. We will measure the net charge of emitted pions to determine if a proton or a neutron was annihilated. The general concept was firstly introduced at Brookhaven [2], and first theoretically investigated for radioactive ions by Wada and Yamazaki [31].

Assuming an antiproton capture cross section of 10^{-16} cm^{-2}, and assuming an antiproton plasma of thickness 10^8 cm^{-2}, every ion at 100 eV will fly through the antiproton cloud 2×10^4 times when trapped for a 10 ms total duration. Assuming that nuclei produced at 1000 s^{-1} are transmitted to PUMA in bunches at 10 ms cycles, the corresponding annihilation rate will be 10 per minute in this particular case. The gain of PUMA is therefore twofold: (i) a specific probe directly sensitive to the proton to neutron density ratio at the nuclear surface, (ii) access to neutron skin information at beam rates as low as a few ions per minute. The design and conception of the extra-high vacuum trap requires exceptionally low background from spurious annihilations. A vacuum of 10^{-17} mbar corresponds to a residual gas density of 0.1 atom / cm^3.

2.3   Theory and interpretation

2.3.1   General concept

Antiprotonic atoms are especially suited to probe the nuclear density at large distance from the nucleus center of mass, since the antiproton-nucleus interaction takes place at about 2 to 2.5 fm outside the half-density radius. After being captured on a Coulomb orbital with principal quantum number $n \gg 1$, the antiprotonic atom decays via X ray and Auger electron emissions towards a state with low n. At this point, the strong interaction becomes important and the Coulomb orbital decays via antiproton-nucleon annihilation. Annihilation is followed by meson emission, mostly pions, conserving charge and momentum. The reconstruction of the total charge of the emitted pions allows determination of the total charge of annihilated particles, that is 0 in case of antiproton-proton annihilation and -1 in case of antiproton-neutron annihilation.

The reaction products of antiproton-nucleon annihilation depend on :
a. Nuclear structure, particularly the ratio of proton to neutron density distribution (our new nuclear physics observable),
b. the antiproton nucleon potential,
c. antiprotonic orbitals which can be calculated from QED with excellent accuracy, and the decay path of the antiprotonic atom,
d. final state interactions originating from the re-interaction of produced pions with the residual nucleus.

In the following, we stress how we will treat the theoretical inputs needed to extract structure information from the measurement (last three items).

2.3.2 antiproton-nucleus interaction

On the theory side, collaborators (G. Hupin, R. Lazauskas, J. Carbonell) will contribute to PUMA in developing several aspects related to antiproton-nucleus systems, as detailed below in the order of increasing difficulty.

1. As a first step, we aim to compare the existing $N\bar{N}$ interaction models. They may be classified in two main groups depending on the way they treat the annihilation process: the optical models or the coupled channel approach. From the optical models side, these are: Dover-Richard [33], Khono-Weise [34], the updated (2009) version of the Paris potential [35] and the recently developed chiral-effective theory inspired potential by Haidenbauer and collaborators [36].
An alternative to the optical model approach is the unitary coupled channel model which can lead to substantial differences in the short range parts of wave functions. We have at our disposal this model developed in another context [37, 38], which will be updated for the low energy physics case.
The main interest of this initial step is to understand the stability of the theoretical predictions in describing the annihilation process in the simplest system including antiparticles: protonium [39]. This implies computation of lower $\bar{p}$-p orbits with the different potentials as well as the corresponding annihilation densities $\gamma_\alpha(r)$ for the lowest states $\alpha = \{LSJ\}$ [39]. These quantities are related to the spatial distribution of the annihilation process, whereas their overlap integrals provide the total width of the state. They can be obtained in terms of the state wave function Ψ_α and the annihilation interaction. In the optical model, it reads

$$\Gamma_\alpha = \int dr \; \gamma_\alpha(r) \qquad\qquad \gamma_\alpha(r) = \mathrm{Im}\left[V_{N\bar{N}}(r)\right] \mid r\Psi_\alpha(r) \mid^2 . \qquad (1)$$

2. A second step consists in computing the $\bar{p}$-A (antiproton-nuclei) Coulomb orbits in the few lightest nuclei for which an exact numerical *ab-initio* solution is accessible. To this aim the Faddeev-Yakubovsky [40, 41] equations in configuration space will be solved. Our present technology allows us to solve A=2,3,4 and 5 problems [41] accounting for the different asymptotic channels. This limits the Faddeev-Yakubovsky approach to the following stable nuclei: ^{2}H, ^{3}H, ^{3}He and ^{4}He. The first results in the $\bar{p} -^2 H$ case, showed however that the calculations are very challenging and it is not clear that this full program could be achieved using the last approach.

After obtaining the exact solution in a few test nuclei, we will make use of another *ab-initio* computation technique for scattering and continuum states, based on the No-Core Shell Model [42]. This method has been successful in describing reactions of a neutron (proton) impinging on a light to medium mass nuclei, up to $A \sim 12$ [43]. This will allow us to study the evolution of low-energy antiproton-nucleus towards heavier and exotic systems aimed by the PUMA project.

At the end of this step we will have computed a set of nuclei for which the widths of the antiprotonic Coulomb orbits can be directly computed with no other approximation

than the ones included when developing fundamental models of the $\bar{N}N$ interaction.

3. Having at our disposal the exact solution for the simplest nuclei, the third and crucial step will consist in validating the results of the $\bar{p}$-nucleus ($\bar{p}$-A) optical potential approach [44, 45, 46], which is one of the key points of the PUMA project. This approach is indeed based on the assumption that the $\bar{p}$-A optical potential is directly related to the nuclear density $\rho(r)$ by means of expressions like

$$V(r) = \frac{2\pi}{\mu_{pA}} \, a_{\bar{p}p} \, \rho(r) \tag{2}$$

where $a_{\bar{p}p}$ is the scattering length and the μ_{pA} denotes the reduced mass of the $\bar{p}$-A system. Furthermore, it assumes that a $\bar{p}$-A potential constructed in this way is able to reproduce the corresponding antiprotonic widths.

It is worth to emphasize that this ansatz has never been tested in the case where all the terms can be exactly computed. To confirm or infirm the validity of (1), and eventually determine what kind of corrections would be required, will constitute a major contribution to the PUMA project.

2.3.3 Antiprotonic orbitals and annihilation site

The location of the annihilation depends on the preceding cascade of the antiprotonic atom. It depends on (i) the population distribution of antiproton annihilation in various atomic states and (ii) the atomic states at which the annihilation occurs, after competition with atomic radiative transitions. Although these quantities can be calculated, the uncertainties related to the cascade should also be estimated. Note that the ions introduced in the trap will be of electric charge $Q = +e$ for most ions. It is expected that a short time after capture ($\sim$ns), Auger electrons are emitted during the decay and the antiprotonic atom is charged, and therefore remains trapped.

We foresee He isotopes to be a special case since a significant portion of He antiprotonic atoms have a lifetime of the order of μs before annihilation [47], meaning that these long-lived antiprotonic atoms will hit the wall of the trap before annihilation, and therefore might not be tagged by pion tracking as good events (this statement depends strongly on the background achieved with PUMA). The left part of Fig. 2 shows the decay pattern of antiprotonic He isotopes with initial charge $Q = +e$, i.e. for $e - \bar{p} - He^{++}$ systems. The right part of Fig. 2 indicates that still a significant portion of the antiprotonic heliums are formed on short lived states and decay rapidly. The portion of antiprotonic He isotopes with short decay will be evaluated and will be considered in determining the measurements to be performed. Note that the initial principal quantum number n of the antiprotonic orbital is given by

$$n \sim n_0 = \sqrt{\frac{M^*}{m_e}}, \tag{3}$$

where M^* is the reduced mass of the $\bar{p}$-nucleus system. This changed from one isotope to another: typically $n \sim 38$ for ^4He and larger for heavier isotopes. One could consider

to introduce He^{++} ions in the trap but we see two important objections to this option: (i) the gas buffer cooling of the ions from the ISOLDE source should lead to a low transmission of $Q = +2e$ ions, (ii) the antiproton capture process is believed to be a three body process where the antiproton is captured after collision with an electron of the atom. The energy loss in the collision with a bound electron of the ion strongly enhances the chances of antiproton capture by the atom.
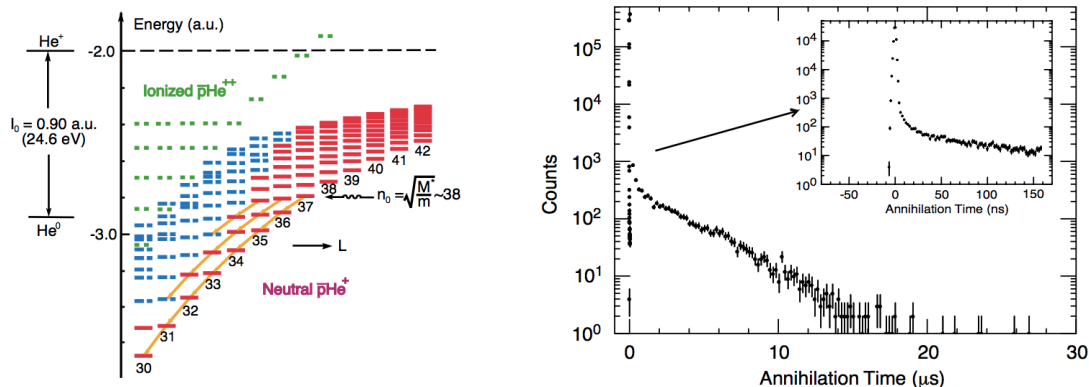

Figure 2: (left) Scheme for the decay of antiprotonc He $\bar{p}He^+$. (right) Lifetime of antiprotonic He. One can see two components: short and long (μs) decays. Figure are taken from [47].

Although the antiprotonic atoms in the trap are initially weakly ionized or neutral, they are surrounded by a rather-low electron density, in comparison to the usual target structure of antiprotonic X- ray experiments. This is expected to make a difference compared to previous experiments with stable nuclei since Auger transitions have a tendency to spread the antiproton cascade to unstreched orbitals (i.e. with lower ℓ values). The Auger transitions among upper atomic levels will be then much reduced during the cascade process because of the small electron-refilling rates. This aspect of the cascade process may not affect greatly the population distribution of antiprotons at the time of the annihilation interaction with nuclear-surface nucleons in lower atomic states. The cascade code to be used was written originally by one of PUMA project members (R. Seki, reference [48]) and was used for the analysis of the last X-ray experiment at LEAR [5].

Next steps In the coming year, the following steps will be performed:
1. Setting and running the existing cascade code, first by the use of an antiproton optical potential with relatively simple, tentatively phenomenological, nuclear surface density distributions. LEAR data will be used to benchmark this step.
2. Improving the simple nuclear surface density distributions by the use of other microscopic density predictions, especially on the proton and neutron contents of the nuclear surface. The uncertainties stemming from the antiprotonic atom forma-
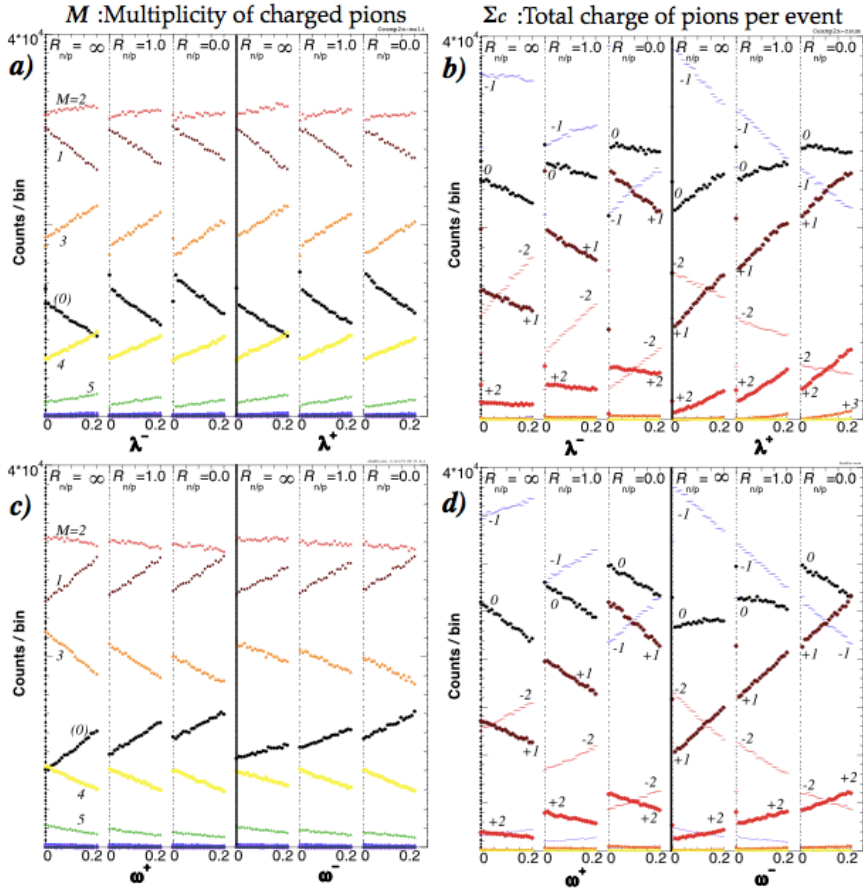
Figure 3: Distortions of the charged-pion production as a function of charge exchange, absorption and proton-over-neutron density ratio. The figure is taken from [52].

tion and decay will be evaluated, first assuming $\bar{p} - A$ potentials of the existing litterature.

2.3.4 Final state interactions

Mesons branching ratios after antiproton-nucleon annihilation have been measured [49, 50]. Main decay channels are listed in Tab. 2. When the annihilated nucleons reside in a nucleus, pions may reinteract with the residual nucleus before being detected with a variety of processes including absorption and charge exchange, generally labelled as Final State Interactions (FSI) [51].

This implies that, even assuming 100% detection efficiency for charged pions, the total charge determination will be biased if FSI are not accounted for. A first simulation of the effect of FSI on measured charge (Σ) and multiplicity (M) is shown in Fig. 3, as a function of different assumptions for the charge exchange (λ) and absorption (ω) probabilities. Fortunately, the FSI can be corrected from the redundancy of the measurement: the observable from PUMA will be the two-dimensional matrix giving the number of events as a function of M and Σ. The matrix contains both the information

antiproton-proton		antiproton-neutron	
Pion final state	Branching ratio	Pion final state	Branching ratio
$\pi^+\pi^-\pi^0\pi^0\pi^0$	0.233	$\pi^-\pi^-\pi^+k\pi^0(k>0)$	0.397
$\pi^+\pi^-\pi^+\pi^-\pi^0$	0.196	$\pi^-k\pi^0(k>1)$	0.169
$\pi^+\pi^-\pi^+\pi^-\pi^0\pi^0$	0.166	$\pi^-\pi^-\pi^+\pi^0$	0.17
		$\pi^-\pi^-\pi^-\pi^+\pi^+k\pi^0(k>1)$	0.12

Table 2: Pion final states for antiproton-proton [49] and antiproton-neutron [50] annihilation with branching ratio >0.1.

on the proton-to-neutron annihilation ratio and FSI effects. At this stage the expected accuracy from these simulations is 5% on the proton-to-neutron annihilation ratio from 5×10^5 antiprotonic atoms assuming 60% detection efficiency of charged pions.

Next steps
1. An analysis method to extract the net annihilation charge from measured pions total charge and multiplicity will be developed and benchmarked on test cases (e.g. light N=Z nuclei, where neutron and proton charge distribution are expected to be the same). To do so, the implementation of antiproton annihilation on nuclei has been recently added into the INCL intranuclear cascade code. Realistic simulations with the design of the PUMA trap will be performed and the accuracy of the developed method to recover the initial proton-to-neutron annihilation ratio will be estimated. A postdoctoral fellow will be hired from September 2018 to focus specifically on this aspect.
2. The algorithm, that can be based on standard fit or more refined neural-network techniques will be implemented using simulated data. The annihilation simulation will be coupled to a realistic simulation of pion detection within the GEANT4 framework. Later on, the algorithm can be applied to extract the ratio of proton over neutron charge for annihilation on light N=Z nuclei (α, ^{12}C), where the ratio is expected to be close to unity. Note that data on different isotopes will allow relative comparison and reduce systematic uncertainties.

2.4 Future perspectives

PUMA might open several other physics opportunities to be further investigated. These measurements will be investigated and fully simulated over the coming two years. We foresee that any new application will require a modification of the detection system and/or trap.

Among others, one could consider the production of neutron rich hypernuclei following the annihilation, the investigation of short range correlations from the annihilation of a high-momentum nucleon in coincidence with the detection of its (high-momentum) partner. The transportation of a large amount of antiprotons would allow their delivery for experiments requiring low-background outside the ELENA area.
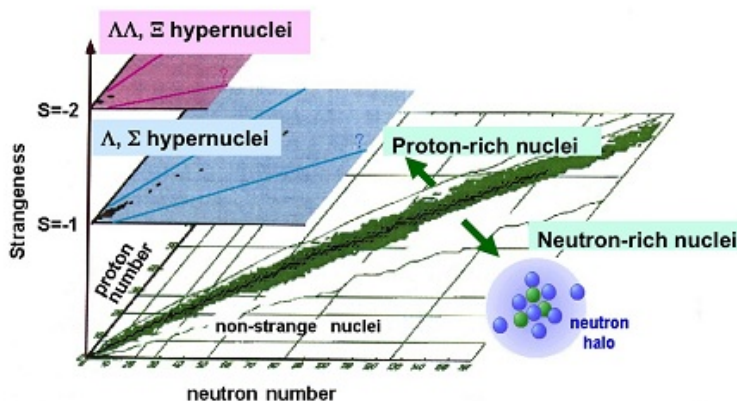
Figure 4: Nuclear landscape extended to the *strangeness* degree of freedom. Few hypernuclei have been observed so far. They are mostly located close to the β stability.

2.4.1 Hypernuclei

Hyperons are baryons with at least one strange quark. The Λ particle with quark constituents *usd* is the lightest hyperon, with mass 1115 MeV/c^2, zero charge, isospin T = 0 and strangeness S = -1, a new quantum number not contained normally inside nuclei. The Λ hyperon is unstable and decays with a lifetime of 263(2) ps, typical of the weak interaction that does not conserve strangeness and makes a free Λ mainly disintegrate into a nucleon-pion system. However, since strangeness is conserved in the strong interaction and the Λ particle is the lightest particle in the family of hyperons, it can stay in contact with nucleons inside nuclei and form short-lived hypernuclei.

The existence and structure of hypernuclei are of great scientific interest. Hypernuclei studies shed a new light on the world of traditional nuclei by revealing new symmetries and new phenomena produced by the additional strangeness dimension. Since their discovery in 1953 [53], hypernuclei have become the most important means to explore the hyperon-nucleon (YN) interaction. Hyperons are free from nucleons' Pauli blocking since they carry an additional strangeness degree of freedom. This feature makes the Λ hyperon, embedded in a hypernucleus, a unique means to study nuclear structure with potentially unexplored capabilities. The gluelike role of a hyperon could shrink the size of the core nucleus [54] and shift the neutron and proton drip lines from their normal limits [55]. Furthermore, the decay of the hyperon from the inside of a nucleus makes it a promising probe for high-density features of nuclear matter. Hyperons might be an important building block of high-density matter such as neutron stars (see for example [56, 57, 58]).

In the past decades, meson (K or π) and electron beams have been used to produce hypernuclei. However, up to now, most of the studied hypernuclei are limited to on/near the β-stability line. In terms of the proton-rich or neutron-rich (exotic) hypernuclei, one of the recent distinguished results was obtained by the FINUDA collaboration [59]. After the analysis of 27 million collision events of $K^- +^6 Li$, they found only three hyperhydrogen $_\Lambda^6 H$ events where significant ΛNN three-body force effect was expected

in theory [60]. Very few exotic hypernuclei have been produced so far while their study would offer a more general understanding of nuclear structure. To explore the properties of hypernuclei lying far from the β-stability line, new techniques aiming at producing exotic hypernuclei with higher intensity are essential. A promising technique is the heavy-ion target and heavy-ion beam induced reaction at high energy pioneered at GSI [61], although this technique may suffer from many other open channels and a complicated reaction mechanism. The technique suffers from the momentum mismatch between the produced Λ and the residual nucleus which should absorb the Λ to for an hypernucleus. Cross sections are therefore small. With PUMA, neutron rich hypernuclei may be formed efficiently from the interaction of a low energy antiprotons and neutron rich nuclei.

Antiproton-nucleus interactions at rest may lead to the production of hypernuclei thanks to the ~ 2 GeV energy available in the center of mass frame. The production of a Λ hyperon from annihilation is interpreted as a two step process when only two-body interactions are considered [62]

$$\bar{p}N \rightarrow K\bar{K} + \pi \text{ followed by } \bar{K}N \rightarrow \Lambda\pi. \tag{4}$$

The low relative energy of the antiproton and the nucleus has the strong advantage to lead to the production of a Λ particle with low momentum relative to the residual nucleus, thus increasing the chances for capture (momentum matching) and formation of a hypernucleus. From past studies, it was found that the formation of hypernuclei can be as high as 2% [63, 64]. Meaning that short lived nuclei produced at 10^5 pps could also be used to synthesise and study hypernuclei. At this stage, we are thinking of investigating possibilities for the gamma spectroscopy of hypernuclei produced in this way.

The low antiproton energy and high luminosity provided at ELENA should allow to further investigate strangeness production from low-energy antiprotons. First studies could be performed at ELENA with stable nuclei. PUMA could provide an efficient way to produce and study neutron-rich hypernuclei at ISOLDE.

Next steps
1. From simulations, estimate the kaon detection efficiency to tag the strangeness production. Determine the kaon detection capabilities of the PUMA setup (momentum and energy loss).
2. Simulate physics cases and estimate the signal over noise in case of gamma spectroscopy.
3. Propose an extension to the design of the apparatus for gamma detection based on high-resolution scintillators.

2.4.2 Short range correlations at low densities

In light of the strong repulsive part of the nucleon-nucleon interaction at short inter-nucleon distances and the existence of collective modes of excitation, it has been anticipated that mean-field based descriptions of nuclei in which nucleons are assumed
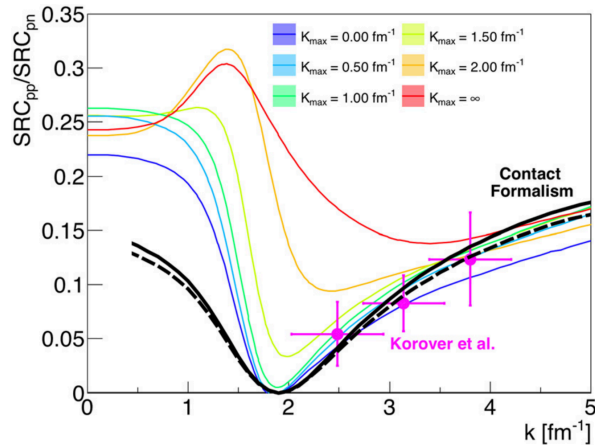
Figure 5: Ratio of pp/pn pairs in ^{4}He as a function of the missing momentum. Figure from [72].

to be independent particles are incomplete. From a systematic study of (e,e'p) proton-knockout reactions from stable nuclei, it was shown that only about 60-70% of the protons contribute to this kind of independent-particle motion [65]. This depletion was interpreted by the existence of correlated pairs of nucleons originating from long-range correlations (LRC) if distances of the order of the nucleus are involved or short-range (SRC) for distances of the size of the nucleon [66]. Such correlations imply that a fraction of the nucleons have momentum high above the Fermi momentum ($q >> 250\,$MeV/c). Experimentally challenging, the unambiguous identification of high-momentum correlated nucleons was achieved only recently using hard-scattering (e,e'pN) reactions with controlled kinematical parameters (see [67] and references therein). Existing data indicate that about 20% of the nucleons are in pairs with large relative momentum q and small center-of-mass momentum Q and that 80% of these correlated pairs are neutron-proton (np) pairs. Within the range of relative momentum probed, between $[300; 600]\,$MeV/c (or $[1.5; 3.0]\,$fm^{-1}), this np-preponderance is explained as steeming from the dominance of the tensor part of the NN interaction at the short distances concerned (1 fm) [68]. This dominance is consistently observed on light and heavy systems from ^{4}He to ^{208}, while a momentum dependence is observed, as illustrated in Fig.5. These first results on SRC-pairs underline that identifying and characterizing how these correlations evolve with nuclear density and isospin asymmetry is of prime interest to constrain the nuclear interaction and could have major consequences on our understanding of nuclear matter in general. For example, this unique enhancement of np-interactions implies that in dense neutron-rich matter, such as neutron stars, protons would be in average at higher momentum, possibly modifying the dynamics and cooling of the system [69]. At lower density, one expects that nucleons are less subject to short-range correlations but clustering [70] may modify this picture. Exclusive hard-scattering experiments using electron beams are still limited to stable nuclei and nuclear saturation density.

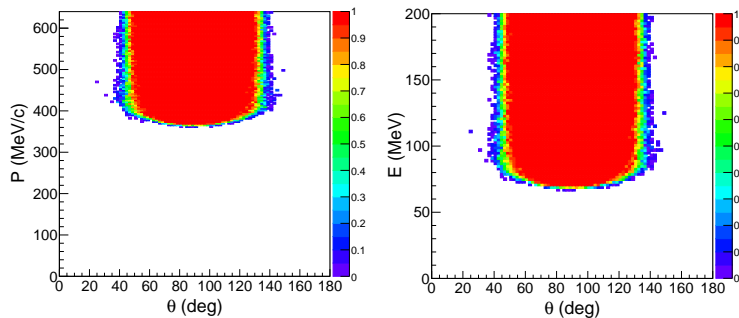With PUMA we propose to study for the first time how these high-momentum correla-

Figure 6: Simulated TPC proton-detection acceptance assuming a 3D-gaussian source ($\sigma_{x,y,z} = 10\,\mathrm{mm}$) and including the budget material from the trap.

tions evolve at low density and with isospin by probing systems with different neutron to proton ratios.

Inferring information on nucleon correlations and momentum distribution from a measurement of (e,e'pN) cross section is ambiguous since those are non-observable quantities and therefore depend on the scale and the scheme of the calculation [71]. The use of a completely different kind of probe may help to disentangle the effect of the reaction process and shed light on the process leading to back-to-back high momentum nucleons emission.

Antiproton-nucleon annihilation at low energy is a process occurring in a controlled peripheral region after antiproton capture on a nucleus. The observables we aimed at providing is the amount of high-momentum protons from correlated pp and pn pairs in a range of relative momentum $q > 1.8\,\mathrm{fm}^{-1}$ for a large variety of nuclear systems. These studies will impulse further formalization of the theoretical building blocks necessary to interpret such measurements. The interpretation will reply on antiproton-nucleon potentials and their momentum dependence. At the momenta involved in short-range correlations, antiproton-proton data exist and should offer a good control of the potentials. Furthermore, stable nuclei data, including deuteron and ^{3,4}He, will be measured and will be used as benchmarks for theory.

The physics program would start with a first commissioning measurement with PUMA at ELENA on ^{3,4}He and ^{12}C, reference cases used by scattering experiments [73]. To this end, we could use first a solid target to avoid difficulties implied by the trapping. After this step, the physics program with trapped ions injected from a stable ion source would focus on the evolution of high-momentum correlations for various stable systems with measurements on ^{4}He, ^{12}C, ^{40}Ar, ^{84}Kr, ^{132}Xe to cover a reasonable range of masses and neutron/proton ratio. Afterwards, the coupling of the PUMA setup to the ISOLDE radioactive ion beam facility would allow to study neutron-rich short-lived nuclei and to explore for the first time the isospin and density dependencies.

As described previously, antiprotons that capture on a nucleus within PUMA will decay

towards inner orbitals to finally annihilate with a nucleon when reaching the region where the density corresponds to a few percents of the nuclear saturation density [74]. This process can be considered as direct which simplifies the mechanism description compared to nuclear reactions at higher energy. While the PUMA physics program focuses on determining the ratio between proton and neutron annihilations in various systems, we propose to determine simultaneously the proportion of events in which a nucleon from a correlated pair is suddenly annihilated by tagging on the detection of the partner high-momentum proton ($q > 350\,\mathrm{MeV/c}$) leaving the nucleus. While annihilation events will be identified by the coincident detection of charged pions in the TPC surrounding the trapping region, we propose to use this TPC to simultaneously detect high-momentum protons originating from correlated pairs and determine their momentum using the curvature of their track in the 4T magnetic field generated by the PUMA solenoid. From preliminary GEANT4 [75] simulations of the setup including material surrounding the trap (cryostat, shielding, etc.) protons in a range from about 350 to 1000 MeV/c can be detected as shown on Fig. 6. This corresponds to a sensitivity window from q=1.8 fm^{-1} to 5 fm^{-1}, competitive with hard-scattering experiments. Due to the very-high segmentation of the Micromegas detection plane of the TPC, a resolution of about $400\,\mu$m is expected on the transverse curvature (sagitta). Analytically, it implies a resolution ranging from 5 to 25% in transverse momentum in the detection range. Proton-pion discrimination would be performed using the energy deposit in the plastic tracker surrounding the TPC.

3 Status and agenda of the technical developments

3.1 Antiproton trapping at ELENA

The PUMA project was made possible thanks to a collaboration with the GBAR collaboration. PUMA will be located at the GBAR experimental site at ELENA for first tests and antiproton trapping. The agreement with the GBAR collaboration to host PUMA was formulated in 2015 at the time PUMA was presented to funding agencies.

GBAR [76, 77] aims at studying the behavior of antimatter in the gravitational field of the earth. The measurement is based on the formation of a $\bar{H}^+$ ion, further cooled down before being ionized to $\bar{H}$. The fall of the resulting $\bar{H}$ is intended to be first measured at a 1 % level. Further improvements of the experiment will target higher accuracy at a later stage. A key part of the GBAR experiment relies on the capture of two positrons by low energy antiprotons. In the experiment, most of antiprotons do not interact with positrons and are sent to a beam dump. PUMA will be located at the beam dump location and will aim at trapping the lost antiprotons.

3.2 Antiproton trap

PUMA aims at building an ion trap that can store antiprotons for a half-life better than a month, the typical time necessary to fill in the trap, transport, re-install and perform collisions with slow radioactive ions. This long term storage can be achieved by avoiding
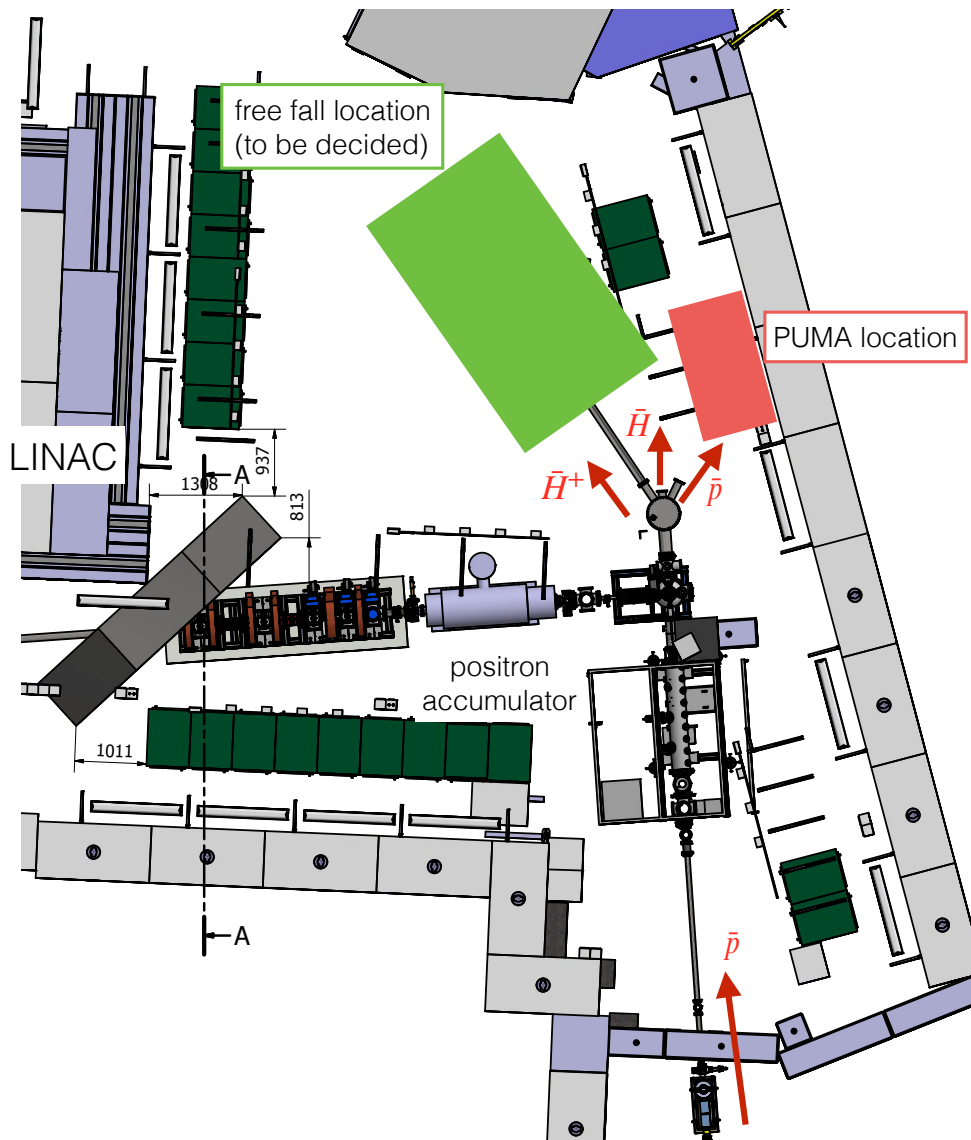
Figure 7: Layout of the GBAR experiment. Courtesy: J.-Y. Roussé (CEA), November 2017.

losses by annihilation on nuclei of the residual gas. The lifetime of the antiprotons is determined by the vacuum in the trap, following the relation

$$P_H(mbar) = 6 \times 10^{-16} T(K)/\tau(days), \tag{5}$$

where P_H is the vacuum in the trap cryostat, T the trap temperature and τ the lifetime of the antiproton cloud. For this purpose, PUMA intends to use a 4 K cryogenic ion trap that can achieve ultra high vacuum better than 10^{-17} mbar.

We will follow the traditional concepts of the Malmberg-Penning trap, where ions are confined by a 4 T magnetic field by a solenoid and electrical potentials from cylindrical electrodes. Both zones (C trap, S trap) will be at the same extreme high vacuum and cryogenic temperatures, and connected by electrodes to transfer ions. The reservoir trap will have large diameter (60 mm) to relax the space charge effect (charge density limited to few 10^7 cm^{-3}) and enable the large number storage of the antiprotons (10^9). The collision trap will consists of 20 mm diameter electrodes, and the two traps will be connected by conical electrodes. The trap will be equipped with non destructive detection circuit as a diagnostic when manipulating the ions and the antiprotons. A pulsed drift tube (PDT) will be placed at the entrance of the trap. Two separated zones offer essential flexibility in the manipulation of the antiproton cloud in the collision trap in terms of electron cooling, length, radius and number of antiprotons. The trap will be designed so that the antiproton density will not exceed $10^7/$ cm^3, already used at other antiproton experiments, to deal with the space charge effect. Once a design of the trap will be finalized, the expected space charge effects will be quantified from simulations. The total trap length is thought to be 800 mm to allow two trapping zones with enough spatial separation. The choice of one unique trap for all functions (storage, transportation, collisions) is motivated by the necessity to maintain a constant magnetic field inside the storage trap during all operations and a perfect alignment of the traps with the magnetic field. These conditions can be ensured in one rigid system, but are more difficult to implement when two solenoids and traps have to be combined together. The trap should also have a size compatible with transportation to radioactive isotope beam facilities, and minimized energy consumption of the cryostat. At this stage of the project, the trap design is still in progress. The simulation of the scheme is ongoing using the SIMION software [78]. The current geometry is shown in Fig. 8.

The main challenge of the system is to obtain ultra high vacuum for long storage of antimatter. Such a regime has already been reached by ion traps for a small number of antiparticles, for example the BASE experiment [79] in which an infinite lifetime ($\geq$ 25 years) for trapped antiprotons has been achieved by combining a sealed trap and cryo-pumping at liquid He temperature [80].

Next steps We intend to build a prototype ion trap at Darmstadt to test our design. We intend to first test the PUMA trap by use of a test solenoid that we will acquire for that purpose. The prototype test will aim at achieving:
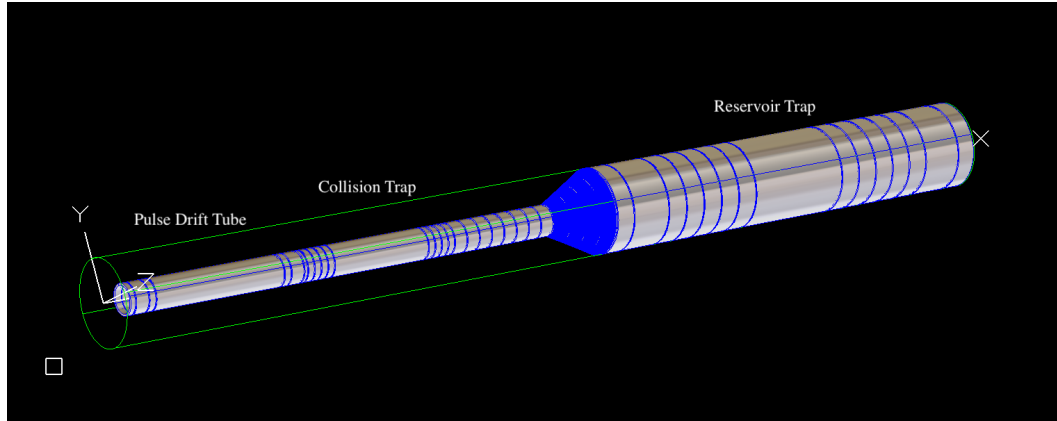1. Ultra high vacuum lower than 10^{-12} mbar (limit of detection without antimatter).

Figure 8: 3D view of the current design of the trap. Electrodes are visible.

2. Temperature as low as 4 K throughout the whole trap.
3. Trapping of protons and destructive/non-destructive detection.
4. Cooling of a proton cloud using sympathetic electron cooling.
5. Apply rotating wall technique to store as many as 10^9 protons.

Step 1 and 2 will be achieved in 2019. Step 3 to 5 will be achieved in 2020.

3.3   Ultra-high vacuum

The objective of PUMA is to maintain a vacuum better than 10^{-17} mbar in the trap for more than a month. This can be obtained by cryopumping. PUMA presents the difficulty that low-energy ions should also be introduced inside the ultra-high vacuum trap, then prohibiting the use of a croystat sealed with a thick entrance window. Two technical solutions, described below, are pursued:

1. cryo-pumping alone,

2. cryo-pumping and a thin nanometric membrane to separate the trap vacuum from the ELENA and ISOLDE vacua.

3.3.1   Cryo-pumping

The cryopumping is active as far as a the trapped molecules or atoms on the cold surface of the trap does not exceed a monolayer of atoms. The necessary time to cover the full cold surface of the inside trap with residual gas atoms gives then the lifetime of the ultra-high vacuum in the trap.

We propose to isolate the ultra-high vacuum of PUMA from the vacuum of ELENA and ISOLDE with a conductance barrier between the two vacua, as illustrated in Fig. 9. Note that long ultra-high vacua have been obtained with this technique at several places, in particular at the Max-Planck Institute of Heidelberg.
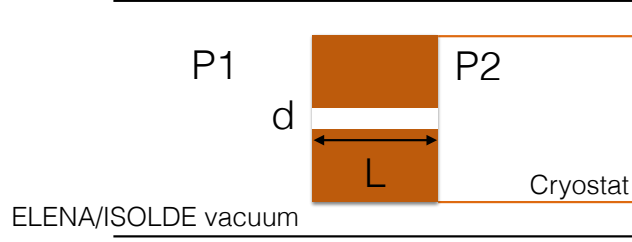
Figure 9: Sketch of the conductance barrier between the ELENA and Isolde vacua and the PUMA ultra-high vacuum maintained by cryopumping of residual gas atoms entering the trap.

The conductance C (m³/s) of a tube as shown in Fig. 9 is given by

$$C = \frac{1}{12} \frac{\pi d^3 \bar{v}}{L},$$ (6)

where $\bar{v}$ is the average velocity of the gas particles in the zone of pressure $P_1 \geq P_2$. $\bar{v}$ can be approximated by

$$\bar{v} = 146 \sqrt{\frac{T}{M}},$$ (7)

where T (in Kelvin) is the temperature of the gas and M is the molecular weight of the gas particle. In the case of PUMA, if one considers $d = 1$ cm, $L = 10$ cm, $M = 2$ (H_2 molecules) and T=70 K, one gets a conductance of $C = 1.8 \times 10^{-2}$ m³/s.

A 4 K surface has such a pumping speed that the above amount of molecules entering the trap are immediately trapped. The main limitation of PUMA in such conditions of cryopumping is the total amount of molecules that it can trap until the surface is saturated.

We focus here on hydrogen, the residual gas molecule which is the most difficult to cryo-pump. The maximum amount of H_2 that the cryopump can absorb for such a non-condensable gas is a function of the vacuum level. A typical value for a 300 cm² pumping surface [81] at 4 K is 1.0×10^{-6} Pa.ℓ. In the case of PUMA we assume a 1-meter long trap with a diameter of 5 cm, giving to a pumping capacity of $\sim 5 \times 10^{-6}$ Pa.ℓ. If one supposes in addition that the vacuum in the trap is kept at 10^{-16} mabr, a conservative value relative to our objectives, the maximum adsordable amount of H_2 is $5 \times 10^7 \ell$. Considering a gas flow from the hole of 1.8×10^{-2} m³/s, as estimated above, the time the 4 K cryostat can keep the vacuum level by cryopumping is estimated to be 310 days, clearly sufficient to achieve the objectives of PUMA.

The above rough estimate only shows that this solution is qualitatively valid. It will be benchmarked with a dedicated setup in the year 2019.

3.3.2 Sealing window for ultra high vacuum

In the case the cryo-pumping is found not to be enough, the PUMA ion trap will be sealed by a thin entrance window. The trap at ultra high vacuum is thought to be separated from a ordinary high vacuum region by a Si_3N_4 20 nm- thick membrane, commercially available. Thicknesses down to 10 nm with proper size are also possible.
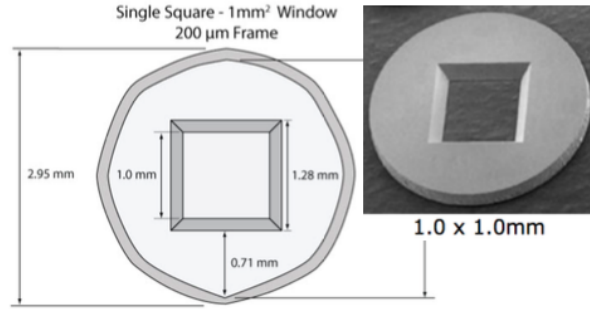

Figure 10: Example of Silicon Nitrite membrane commercially available.

Handling such thin membranes is challenging. PUMA will rely on a collaboration with J. Wieser, who developed in collaboration with his colleagues at TUM (Munich) methods to solder or glue such membranes onto metallic frames [82]. In past experiences, he already produced 2×2 mm^2 membranes with a thickness of 300 nm onto a Si wafer which was itself soldered onto an Invar flange. The choice of materials require a specific consideration of thermal expansion coefficients. J. Wieser and his colleagues exploited this technology to develop electron-induced X-ray systems. So far they showed that a 300 nm window can handle several bar of pressure difference. He expects that a 20 nm window of 2×2 mm^2 could handle several mb of differential pressure, which would make the pumping across the membrane rather easy. They also demonstrated that such windows (300 nm were tested) could resist when cooled down to 70 Kelvin. This information is extremely encouraging. We recently received a first test window (300 nm mounted on an Invar flange) from J. Wieser and will perform our first tests with it.

A high transmission of antiprotons can be achieved through such a thin window. Energy loss of very low-energy ions, protons and antiprotons in solid foils has been studied and reproduced by calculations. For antiprotons, the transmission is estimated to be better than 90 %. Both antiprotons and, in a second phase, ions, should go through the entrance window with minimal loss. This implies a minimum kinetic energy at the exit of the thin entrance window to minimise angular and energy straggling, as well as losses from interactions. On the other hand, the antiprotons and ions have to be trapped downstream of the entrance window, requiring a very low kinetic energy. We foresee tuning the kinetic energy of antiprotons and ions before entering the trap so that their kinetic energy at the exit of the window is about 3 keV. Their kinetic energy will then be slowed down by a decelerating electric potential inside the trap using a dedicated pulsed drift tube as explained above.

A Monte-Carlo simulations was performed using SRIM [83] as a first estimation. For ^{11}Li ions at 4 keV passing through 15-nm Si_3N_4 membrane, the transmission was estimated to be 93 %. The energy loss was 1.7 keV in average with straggling of 0.8 keV in standard deviation (Fig. 11 top). The angular straggling was 0.3 rad in average (Fig. 11 bottom). Note that the magnetic field of the trap will focus the incoming ions into the antiproton trap, however not considered in the present simulation. After passing through the entrance window, the charge state distribution also depends on the ions' atomic charge. The foreseen window thickness corresponds to the order of a hundred of mean free paths for charge exchange. Therefore the final charge state of ions should depend on atomic processes occurring in the window and on the ion velocity at the exit of the window. Incoming ions will be singly charged. At 4 keV exit kinetic energy, phenomenological models predict that 40 % Mg ions exit the entrance window with charge +1, others are mostly neutralized which are then lost for trapping. As described below, a series of measurements is foreseen to benchmark the charge state distribution of very low-energy ions through nano-metric Si_3N_x membranes.
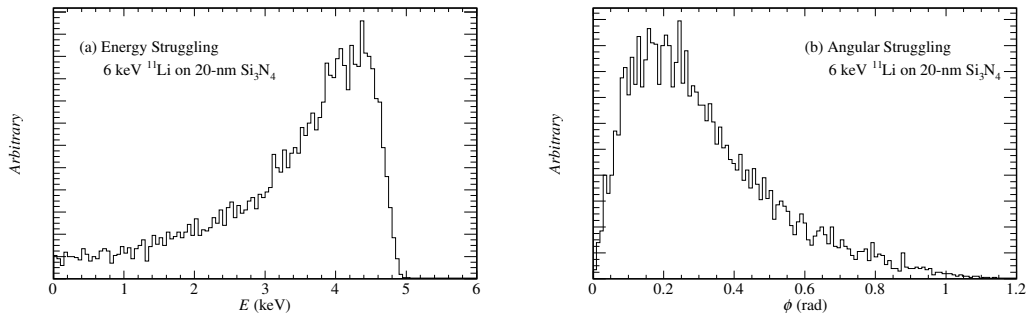

Figure 11: A Monte-Carlo simulation of ^{11}Li ion with the energy of 4 keV passing through 15 nm.

The design of the PDT is ongoing using SIMION. The PDT will be located in the shoulder of the solenoid field to counterpart the angular spread due to the deceleration. In order to trap, the PDT should be able to decelerate antiprotons of 3-4 keV down to 10-40 eV. We made a realistic assumption of an emittance from ISOLDE, axial length of 100 nsec, energy resolution of 30 eV. However, the emittance is significantly broadened by energy and angular straggling in the sealed window. For a 8 keV ^{11}Li beam passing through the 50 nm Si_4N_3 window, the energy straggling is estimated to be 300 eV in sigma with 3000 keV mean value, and the angular spread is 27.2 mrad in sigma. Although these values are not benchmarked and need to be measured, the simulation of the PDT was performed with these inputs. The length of the PDT tube is determined to be 150 mm so that the plateau of the electric field within the tube is long enough for the ISOLDE emittance. Outputs are shown in Fig. 12 with (B = 4 T, top panel) and without (B = 0 T, bottom panel) magnetic field. One can see that the strong focusing effect of the magnetic field counteracts the large angular straggling. The particles with lower axial energy might not have enough kinetic energy to overcome the potential barrier and are then reflected

backwards. Large energy straggling will also limit the transmission efficiency since low energy particles may not overcome the electric potential if set too high. The choice of the PDT deceleration potential will then be a trade off between a strong deceleration and a large transmission.
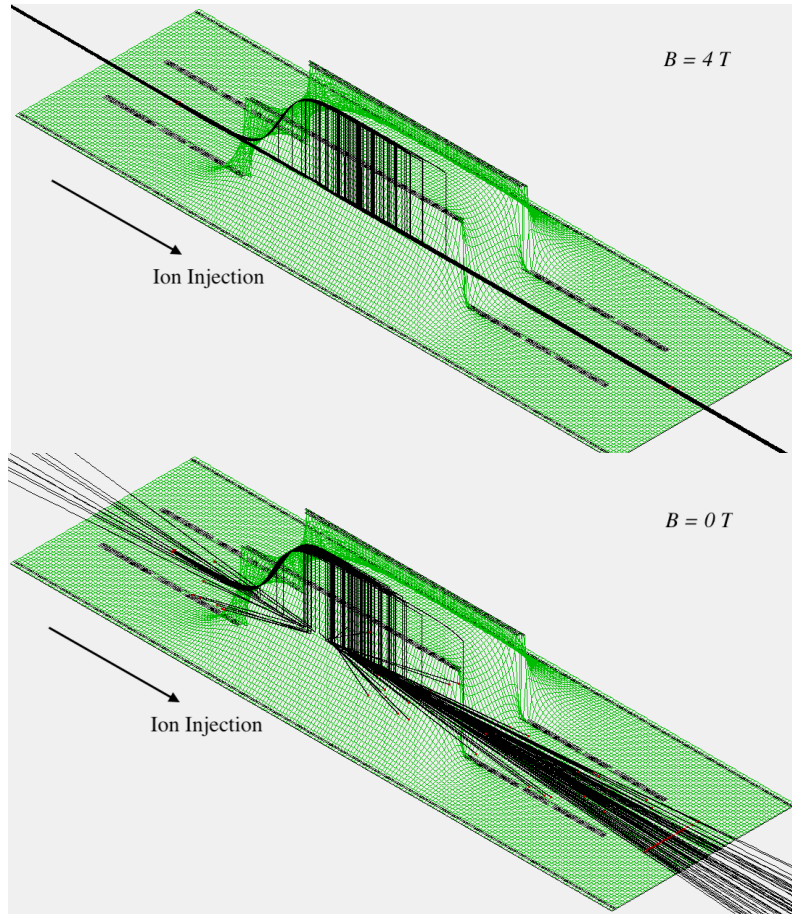

Figure 12: Simulation of ^{11}Li ion trajectories (black lines) flying through the PDT with (top) and without (bottom) magnetic field. The focusing effect of the magnetic field of the solenoid is visible. The surface of electric potential is shown (green).

Next steps The cryogenics and mechanical parts for membranes of thicknesses lower than 100 nm should be demonstrated. The following steps are foreseen in the coming 18 months.

1. Test a 300-nm Si_3N_x window at 4 K.

2. Soldering the window into the vacuum flange. Choice of material of the flange will be tested. First we will mount a 300-nm Si_3N_x window on a Cu flange.

3. Same as above for membrane thicknesses of 100 nm, 50 nm, 20 nm, 10 nm.

4. Determine which pressure differentials the sealing membrane can support. Test pumping across thin membranes (50, 20, 10 nm).

5. Cool down cryostat to 4 K with thin membranes mounted to test if the window survives the thermal stress.

In addition, energy loss, straggling and charge state distribution of low energy ions through Si_3N_x membranes should be measured to benchmark model predictions. In case of significant deviation, new phenomenological models will be developed for PUMA. A dedicated test bench will be developed, and the following will be tested

1. Energy loss of ions from mass A=1 to A=50 will be measured for different incident energies and membrane target thicknesses.
2. Angular straggling will be determined.
3. Charge distribution after the membrane will be measured.
4.The resistance of the membranes to high ion flux will be determined.
5. Residual gas condensation on the membrane surface will be measured from energy loss variation with time.

3.4   Solenoid

The solenoid should have a size compatible with transportation and minimum energy consumption. The necessary magnetic field strength for the ion trap is expected to be about 4 T at the center. This field strength is also sufficient for the tracking efficiency and momentum sensitivity of emitted pions, both determined from the curvature of the tracks. It will also be designed with reduced external field to comply with the agreement with the surrounding experiments at ELENA. In order to meet with those requirements, the solenoid will consist of a superconducting coil equipped with both active and passive shielding. We are considering a homemade design, to be discussed in detail in the next section.

The transportable Penning trap is a central part of the PUMA experiment. In order for the trap to confine charged particles in closed orbits, a quadrupolar electric field, as well as a homogeneous magnetic field, are required [84]. In addition to trapping purposes, an homogeneous magnetic field is also required for the detection of collisions between low-energy antiprotons and radioactive nuclei. Therefore, the design of a magnet generating a 4 T induction field with a high homogeneity is a critical part of the PUMA project.

3.4.1   Specifications

The magnetic induction that must be generated by the PUMA magnet is submitted to many constraints, which can be categorized into three groups:
1. the homogeneity inside the magnet,
2. the magnitude of the exterior field,
3. the gradient of the exterior field along the gravity axis.

This last constraint on the gradient is a requirement of the neighboring GBAR experiment located at ELENA [76, 77]. Concerning the first constraint, the PUMA project requires two homogeneity regions, $\pm0.2\%$ and $\pm5\%$, which are described in Table 3. Regarding the exterior field, the requirements are given in Table 4 for a distance of 3 m from the magnet.

Table 3: Homogeneity region of the PUMA magnet

Volume description	Homogeneity
800 m long cylinder, 25 mm radius	±0.2%
800 m long cylinder, 110 mm radius	±5%

Table 4: Constraints on the exterior field at a distance of 3 m from the magnet.

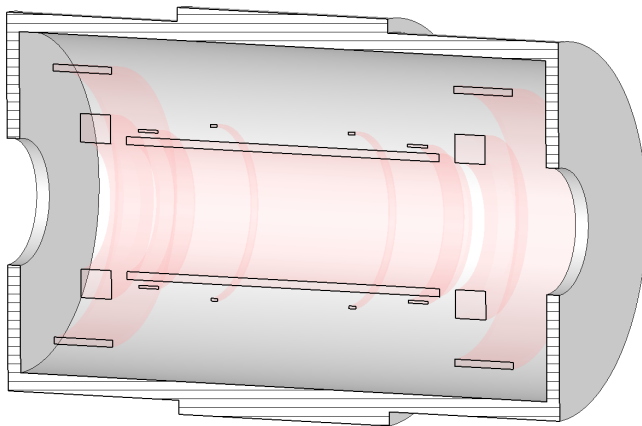| Description of the constraint	Maximum value	Additional comment
Magnitude of the field	200 μT	
Magnitude of the gradient	20 μT/m	Measured at 45° of the magnet axis and along the gravity axis

Figure 13: Three-dimensional view (axial cut).

The magnet of the PUMA Penning trap was designed by means of numerical optimization technique, as it is the case nowadays for almost all high performance electrical machines. In particular, we followed the two-step approach proposed in [85], then introduced a third stage, in order to take the passive shielding into account.

Once an optimal solution is found, the passive shielding is introduced. In order to satisfy the maximal length constraint, the passive shielding must be placed close to the coils, which modifies significantly the field homogeneity. Therefore, a third optimization step is required, which relies on the same setup as for the previous stage, except for the non-linearity introduced by the saturation of the passive shield.

The methodology described in the previous section has been applied to design the magnet of the PUMA Penning trap, and has led to the design depicted in Fig. 13. It requires approximately 240 kg of niobium for the coils and 1500 kg of iron for the passive shield. This large amount of magnetic material is explained by its proximity with the coils. Therefore, in order to limit the saturation, a thick shield is required. Finally, and for illustration purposes, Figure 14 shows the spacial distribution of $\|\mathbf{B}\|$ for an homogeneity of ±0.15% (i.e. within the 0.2% specifications).
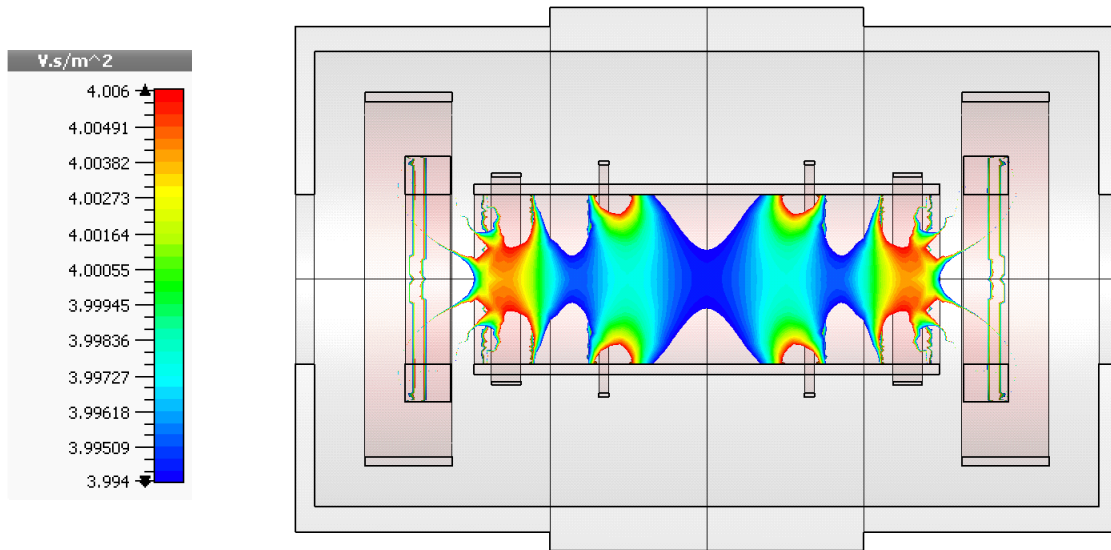
Figure 14: Magnitude of the magnetic induction: $\pm 0.15\%$ homogeneity for the 25 mm radius region.

Next steps The above specifications and design are the basis for a Call for Tender under preparation at TU Darmstadt. We expect the solenoid to be ordered by the end of 2018 and ready for operation within 16 months.

3.5 Radioactive ions

Radioactive ions are produced at ISOLDE from the interaction of protons from the PS booster and the ISOLDE production target. Different ion sources have been developed at ISOLDE and allow the extraction of a large range of elements. The low-energy branch of ISOLDE will be used. Produced low-energy ions will be cooled and bunched. They will then be delivered at a kinetic energy of few keV to the experiment. Several technical solutions, including the use of the ISCOOL RFQ cooler with fast extraction, are investigated. The experimental location for PUMA at ISOLDE could be the beam lines LA1 or LA2 dedicated for traveling apparatus, although other options are also considered at this stage.

Currently, the ISOLDE facility can deliver radioactive beams quasi continuously (chopped by opening and closing an electrostatic beam gate) through one of the magnetic mass separators or as cooled and bunched beams if the ISCOOL ion cooler and buncher within the HRS branch is used.

Depending on the demands of the individual experiment, a cooler-and-buncher device is able to extract the bunched beams either with small energy spreads and a wider time
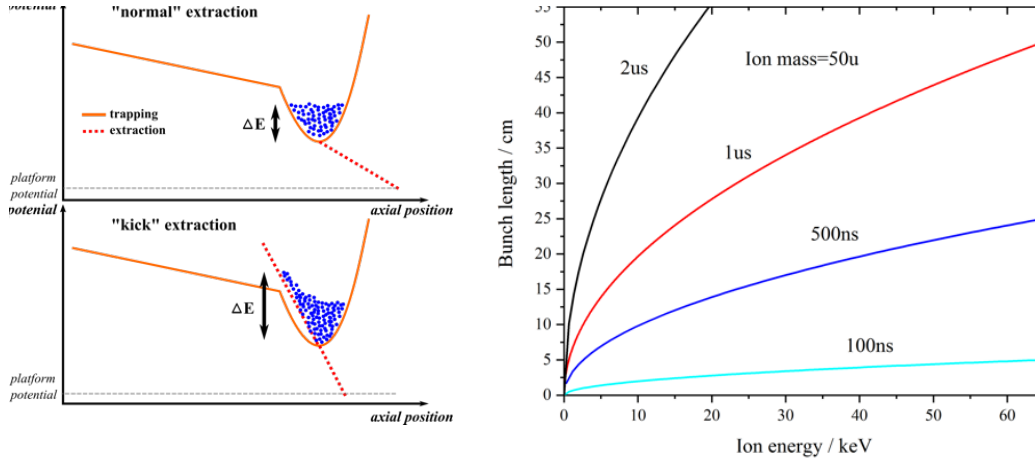
Figure 15: (left) Different extraction modes from an RFQ cooler and buncher. (right) Geometrically bunch length as a function of the ion energy for different temporal time widths.

spread or vice versa. The left side of figure 15 schematically shows the different modes of extraction and right side additionally presents how the geometrical width of the beam depends on the ion energy for different temporal bunch widths. It is important that the length of the bunched beam can be controlled, so that it can fit within a cylindrical electrode to finally decelerate it sufficiently enough by the potential lift technique, so that it can be introduced into the PUMA setup. This technique will have to be implemented independently of the currently available infrastructure and will thus be part of the PUMA setup. Further characterization of the ISCOOL is very important to determine the need of additional beam manipulation devices and ion optics. For the future PUMA measurement campaign, the purity of the beam is of utmost importance. That is why it will greatly profit form the developments currently underway within the MIRACLS project and in feasibility and design studies for a potential future MR-ToF for ISOLDE. Both aim to develop of a Multi-Reflection Time-of-Flight Mass Separator (MR-ToF MS) at 30 kV ion energy reaching a mass resolving power of several 1E5 within few milliseconds. The higher beam energy will improve the ion throughput, enable us to run with a factor of 4 improved duty cycle compared to the MR-ToF MS at ISOLTRAP. That device will allow the fast and efficient identification and cleaning of the beam coming from ISOLDE. The deceleration of the incoming beam, to be able to inject it to the PUMA setup, will, as already mentioned, either be done by means of the potential lift technique or by means of a crown-shaped electrode which has been successfully tested recently under beam time conditions by the VITO collaboration. A schematic view of the electrode and its potential distribution on axis are presented in figure 16.

Further developments regarding a cryogenic buncher system that the MIRACLS collaboration are considering, will decrease the thermalisation time of the ions within the buffer gas environment of the RFQ greatly and additionally decreasing the turn-around time of the ions which will further decrease the time needed to reach a certain mass resolving power. The presence of a new, dedicated buncher will also allow us to take beam from
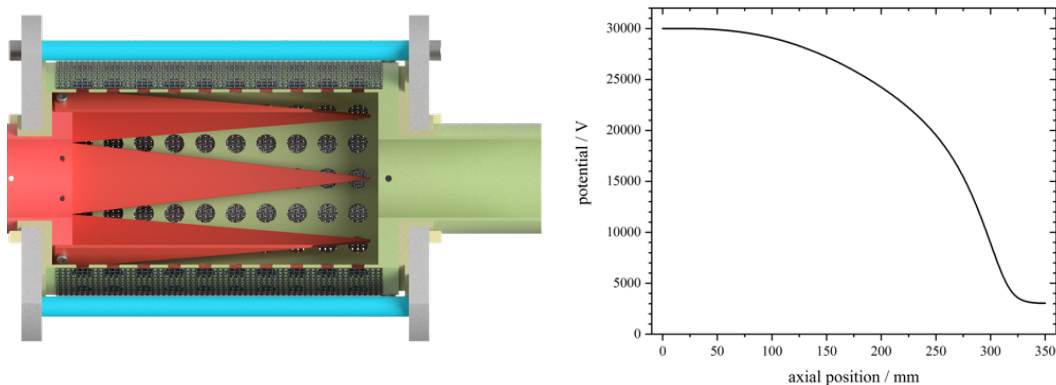
Figure 16: (left) Schematic cut CAD view of the deceleration "crown-cylinder" electrode. (right) Potential distribution on axis of the deceleration electrode from 30kV to 3kV.

both target stations.

3.6   Detection of pions

The principal PUMA detection system consists of an annular TPC surrounded by a plastic scintillator barrel, located around the collision trap. A second plastic scintillator barrel surrounds the reservoir trap. The challenges accompanying this project are to maximize the compact active volume in the TPC within the small volume available in the solenoid and yet have a sufficient efficient space available for the scintillator barrel. Apart from low straggling, an important facet of this project is that the detection has to be highly reliable. Namely the conceptual design requires not to have any intervention on the detection over the whole operational life-time of the system.

The conceptual design reached as of today has yielded a TPC where the cathode, field cage and gas anode have a noncomplex design with low sparking risks and a reduced number point-to-point contacts. Nevertheless, the design allows access to the principle elements (eg electronic connections) and permits repair should it be proven necessary.

Simulations of the field cage are in progress. The objective is to maximize the uniformity of the electric field within the active volume. The principle difficulties lie in the interface between the anode and field cage. Inhomogeneities are being corrected through the introduction of electrodes. The work is progressing and we have reasonable results. This work should be completed in 2-3 months time.

The field cage and its interface to the anode and cathode is close to being finalized. It is a novel design in its simplicity, robustness and low mass. To date the E-field simulations have proven the design rather positive. A reduced sized model has been built to prove the mechanical principles. A large fraction of the mechanical study has been completed and now awaits spark simulation studies to be performed. An offer has been received by

MPGD (CERN) Section EP-DT-EF for detail design and construction of the TPC. The offer has been accepted under modification arrangements. The design work should be completed in 2 months of working time once geometries of the solenoid and beam line are finalized.

Gas tightness will be secured via O-rings. Specifications are set at a maximum of 20 ppm contamination through leaking at 0.2% above atmospheric pressure. The gas mixture choice will be most likely be a standard mixture but which will favor good charge resolution. Gas refreshing and flow with the present design will be studied to avoid laminar flow which leaves pockets of contaminated gas. The anode PCB pad-plane will be the air-to-gas interface. No priority has yet been set on the gas, gas handling system etc. However, specifications have been set.

The chosen gas amplifier is a Micromegas pad plane. The choice rests on the mechanical simplicity and robustness of the Micromegas concept. The gain for pions will be sufficient. To enhance the durability, a resistive coating (DLC) will be applied between the mesh and the pad plane. This reduces the spark frequency and hence increases the longevity of the detector electronics. The pre-amplification stages need not be protected using this technique. The PCB substrate will carry approximately 5000 channels with a density of approximately 25 pad/cm^2. The disposition of the pads and connectors to the electronics has been chosen and awaits final inspection.

A full simulation to include the electric and magnetic field will be needed to confirm the event and electron drift reconstruction based on the chosen pad plane geometry, gas amplification and electronics. This work is in progress. The construction of the TPC will follow the study of the issuing report which be made available in approximately 4 months.

The TPC will be tested using cosmic rays and sources for approximately 9 months to establish reliability and performance. Following positive results the TPC and barrels will be installed at CERN with the full setup.

The conceptual design of the scintillator barrels and their integration around the TPC has been done by MPGD (CERN). The barrel will have 12 plastic slabs read off by two SiPMs at either end. The electronics channels to read the SiPMs will be the same as that of the TPC and fully integrated with those of TPC. The GET system will be deployed to test the SiPMs. The final detailed design of the mechanical design and assembly/integration with the TPC will be the responsibility of TUD. The same design but in a smaller configuration will be deployed for the reservoir section. It is considered that the whole barrel design work and assembly should be completed in approximately 6 -8 months.

Next steps Full operation of the complete detection system is expected for early 2020. The main milestones are:
1. The final design of the TPC will be set once the dimensions of the solenoid are settled. We expect a final design by the end of 2018.

2. The detector and the plastic scintillator array should be finalized in 2019.

4 Collaboration and resources

The PUMA collaboration is under construction. Twenty collaborators from seven universities and institutes are officially involved in the project: TU Darmstadt, CEA, CERN, RIKEN, IPN Orsay, RCNP and IPHC. Discussions with other groups are ongoing. Four additional positions at TU Darmstadt (2 PhD, 1 postdoc and 1 staff) should be open in the coming year with a main focus on PUMA.

A series of meetings are foreseen in the near future. From 2019, PUMA collaboration meetings will be held twice a year. Two workshops dedicated to Antiproton-nucleus interactions at low energy and related phenomena" are foreseen in 2019. Once ECT⋆ proposal was recently submitted and will cover both experimental and theoretical aspects. The second workshop will focus on theoretical methods to describe antiproton-nucleus systems.

The development of PUMA is funded to a large extend by an ERC grant for five years over the period 2018-2022 [86] and by TU Darmstadt. A new technical laboratory is expected to be created at TU Darmstadt from 2019 with additional resources. In particular, the laboratory will be equipped with a test solenoid and a stable ion source line for the development of PUMA in the coming years. The detectors of PUMA will also be tested in the laboratory.

References

[1] Letter of Intent, CERN-SPSC-I-247 (2017).

[2] W. N. Bugg et al., Phys. Rev. Lett. **31**, 475 (1973).

[3] J. Eades and F.J. Hartmann, Rev. Mod. Phys. **71**, 373 (1999).

[4] S. Wycech et al., Phys. Rev. C **54**, 1832 (1996).

[5] R. Schmidt et al., Phys. Rev. C **60**, 054309 (1999).

[6] B. Klos et al., Phys. Rev. C **76**, 014311 (2007).

[7] P. Lubinski et al., Phys. Rev. C **57**, 2962 (1998).

[8] A. Trzcinska et al., Phys. Rev. Lett. **87**, 082501 (2001).

[9] E. Widmann, Phys. Scripta, T166 (2015).

[10] E. Kugler et al., Nucl. Instr. Meth. B **70**, 41 (1992).

[11] I. Tanihata et al., Phys. Rev. Lett. **55**, 2676 (1985).

[12] P.G. Hansen and B. Jonson, Europhys. Lett. **4**, 409 (1987).

[13] P.G. Hansen, A.S. Jensen and B. Jonson, Ann. Rev. Nucl. Part. Sc. **45**, 591 (1995).

[14] T. Nakamura et al., Phys. Rev. Lett. **112**, 142501 (2014).

[15] N. Kobayashi et al., Phys. Rev. Lett. **112**, 242501 (2014).

[16] S. Mizutori et al., Phys. Rev. C **61**, 044326 (2000).

[17] M. Grasso et al., Phys. Rev. C **74**, 064317 (2006).

[18] J. Terasaki et al., Phys. Rev. C **74**, 054318 (2006).

[19] V. Rotival and T. Duguet, Phys. Rev. C **79**, 054308 (2009).

[20] V. Rotival, K. Bennaceur and T. Duguet, Phys. Rev. C **79**, 054309 (2009).

[21] I. Hamamoto, Phys. Rev. C **69**, 041306(R) (2004).

[22] I. Hamamoto, Phys. Rev. C **76**, 054319 (2007).

[23] I. Hamamoto, Phys. Rev. C **81**, 021304(R) (2010).

[24] S. Abrahamyan *et al.*, Phys. Rev. Lett. **108**, 112502 (2012).

[25] M. H. Mazhzoon *et al.*, Phys. Rev. Lett. **119**, 222503 (2017).

[26] C. M. Tarbert *et al.*, Phys. Rev. Lett. **112**, 242502 (2014).

[27] A. Tamii *et al.*, Phys. Rev. Lett. **107**, 062502 (2011).

[28] S. Typel, Phys. Rev. C **89**, 064321 (2014).

[29] S. Typel et al., Eur. Phys. J. A **50**, 17 (2014).

[30] G. Hagen et al., Nature Physics (2015), doi:10.1038/nphys3529.

[31] M. Wada and Y. Yamazaki, Nucl. Instr. Meth. B **214**, 196 (2004).

[32] J. S. Cohen, Phys. Rev. A **69**, 022501 (2004).

[33] C. B. Dover and J. M. Richard, Phys. Rev. C **21**, 1466 (1980).

[34] M. Kohno and W. Weise, Nucl. Phys. A **454**, 429 (1986).

[35] B. El-Bennich, M. Lacombe, B. Loiseau and S. Wycech, Phys. Rev. C **79**, 054001 (2009).

[36] L.-Y. Dai, J. Haidenbauer, U.-G. Meißner , JHEP 1707, 078 (2017).

[37] O.D. Dalkarov, K.V. Protasov, J. Carbonell, Sov. J. Nucl. Phys. **52**, 1052 (1990).

[38] J. Carbonell, K.V. Protasov, O.D. Dalkarov, Phys. Lett. B **306**, 407-410 (1993).

[39] J. Carbonell, G. Ihle, J.M. Richard, Z. Phys. A 334, 329-341 (1989).

[40] R. Lazauskas, J. Carbonell, Phys. Rev. C **70**, 044002 (2004).

[41] R. Lazauskas, Phys. Rev. C **97**, 044002 (2018).

[42] P. Navrátil, S. Quaglioni, G. Hupin, C. Romero-Redondo and A. Calci, Phys. Scr. **91**, 053002 (2016).

[43] A. Calci, P. Navrátil, R. Roth, J. Dohet-Eraly, S. Quaglioni, and G. Hupin, Phys. Rev. Lett. **117**, 252501 (2016).

[44] S. Wycech, Nucl. Phys. A **561**, 607 (1993).

[45] C.J. Batty, E. Friedman, A. Gal, Phys. Rep. **287**, 385 (1997).

[46] R. Schmidt et al Phys. Rev C **58**, 3195 (1998).

[47] T. Yamazaki *et al.*, Phys. Rep. **366**, 183 (2002).

[48] M. Leon and R. Seki, Phys. Lett. B **48**, 173 (1974).

[49] C. Ghesquiere, Symposium on Antinucleon-Nucleon Interactions, CERN (1974).

[50] S. J. Orfanidis and V. Rittenberg, Nucl. Phys. B **59**, 570 (1973).

[51] D.Mancusi *et al.*, Eur. Phys. J. A **53**, 80 (2017).

[52] M. Wada and Y. Yamazaki, private communication (unpublished).

[53] M. Danysz and J. Pniewski, Philosophical Magazine Series 7, 348 (1953).

[54] K. Tanida *et al.*, Phys. Rev. Lett **86**, 1982 (2001).

[55] C. Samanta *et al.*, J. Phys. G: Nucl. Part. Phys. **35**, 065101(2008).

[56] V. A. Ambartsumyan and G. S. Saakyan, Sov. Astron. **4**, 187 (1960).

[57] S. Balberg and A. Gal, Nucl. Phys. A **625**, 435 (1997).

[58] D. Lonardoni, A. Lovato, S. Gandolfi and F. Pederiva, Phys. Rev. Lett. **114**, 092301 (2015).

[59] M. Agnello *et al.*, Phys. Rev. Lett **108**, 042501 (2012).

[60] Y. Akaishi, Prog. Theor. Phys. Suppl. **186**, 378 (2010), and references therein.

[61] T.R. Saito *et al.*, Nucl. Phys. A **835**, 110 (2010); T.R. Saito *et al.*, Nucl. Phys. A **881**, 218 (2012).

[62] M. Rey-Campagnolle, Nuovo Cim. **102**, 653 (1989).

[63] G. T. Condo, T. Handler and H. O. Cohn, Phys. Rev. C **29**, 1531 (1984).

[64] F. Balestra *et al.*, Phys. Lett. B **194**, 192 (1987).

[65] L. Lapikas, Nucl. Phys. A **553**, 297 (1993).

[66] W. H. Dickhoff and C. Barbieri, Prog. Part. Nucl. Phys. **52**, 377 (2004).

[67] O. Hen, G. A. Miller, E. Piasetsky and L. B. Weinstein, Rev. Mod. Phys. **89**, 045002 (2017).

[68] R. B. Wiringa, R. Schiavilla, S. C. Pieper and J. Carlson, Phys. Rev. C **89**, 024305 (2014).

[69] M. M. Sargsian, J. Phys.: Conf. Ser. **496**, 012007 (2014).

[70] J. P. Ebran, E. Khan, T. Niksic and D. Vretenar, Nature **487**, 341 (2012).

[71] S. N. More, S. K. Bogner and R. J. Furnsthal, Phys. Rev. C**96**, 054004 (2017).

[72] R. Weiss *et al.*, Physics Letters B **780**, 211 (2018).

[73] R. Subedi *et al.*, Science **320**, 1476 (2008).

[74] R. Schmidt *et al.*, Phys. Rev. C **58**, 3195 (1998).

[75] S. Agostinelli *et al.*, Nucl. Instr. Meth. A **506**, 250 (2003).

[76] GBAR collaboration, "Proposal to measure the gravitational behaviour of antihydrogen at rest", CERN-SPSC-2001-029 / SPSC-P-342 (2011).

[77] P. Pérez *et al.*, Hyperf. Int. **233**, 21 (2015).

[78] D. A. Dahl, Int. J. Mass Spectrom. **200**, 3 (2000).

[79] S. Ulmer *et al.*, http://base.web.cern.ch, Technical Design Report BASE, CERN (2013).

[80] C. Smorra *et al.*, Nature **550**, 371 (2017).

[81] ULVAC catalogue.

[82] J. Wieser *et al.*, Eur. Phys. J. D **48**, 383 (2008).

[83] J. F. Ziegler *et al.*, "The Stopping and Range of Ions in Solids", www.SRIM.org (2008).

[84] L. S. Brown, G. Gabrielse, Rev. Mod. Phys. **58**, 233 (1986).

[85] W. Wu, Y. He, L.-Z. Ma, W.-X. Huang, and J.-W. Xia, Chin. Phys. C **34**, 978 (2010).

[86] ERC Consolidator Grant (2018-2022), PUMA, A. Obertelli.